IN 34
58-38
P-11

NASA Technical Memorandum 105372
AIAA-92-0363

Self-Pressurization of a Spherical Liquid Hydrogen Storage Tank in a Microgravity Environment

C.S. Lin
Analex Corporation
Brook Park, Ohio

and

M.M. Hasan
Lewis Research Center
Cleveland, Ohio

Prepared for the
30th Aerospace Sciences Meeting and Exhibit
sponsored by the American Institute of Aeronautics and Astronautics
Reno, Nevada, January 6-9, 1992

NASA

(NASA-TM-105372) SELF-PRESSURIZATION OF A SPHERICAL LIQUID HYDROGEN STORAGE TANK IN A MICROGRAVITY ENVIRONMENT (NASA) 11 p
N92-14323
CSCL 20D
Unclas
G3/34 0058238

SELF-PRESSURIZATION OF A SPHERICAL LIQUID HYDROGEN STORAGE TANK IN A MICROGRAVITY ENVIRONMENT

C.S. Lin*
Analex Corporation
Brook Park, Ohio 44142

and

M.M. Hasan*
National Aeronautics and Space Administration
Lewis Research Center
Cleveland, Ohio 44135

E-6759

Abstract

Thermal stratification and self-pressurization of partially filled liquid hydrogen (LH_2) storage tanks under microgravity condition is theoretically studied. The tank is spherical and is subjected to a uniform and constant wall heat flux. It is assumed that a vapor bubble is located in the tank center such that the liquid-vapor interface and tank wall form two concentric spheres. This vapor bubble represents an idealized configuration of a wetting fluid in microgravity conditions. Dimensionless mass and energy conservation equations for both vapor and liquid regions are numerically solved. Coordinate transformation is used to capture the interface location which changes due to liquid thermal expansion, vapor compression, and mass transfer at liquid-vapor interface. The effects of tank size, liquid fill level, and wall heat flux on the pressure rise and thermal stratification are investigated. Liquid thermal expansion tends to cause vapor condensation and wall heat flux tends to cause liquid evaporation at the interface. The combined effects determine the direction of mass transfer at the interface. Liquid superheat increases with increasing wall heat flux and liquid fill level and approaches an asymptotic value. A simplified correlation is developed for the maximum wall superheat as a function of system parameters using the numerical results.

Nomenclature

a	acceleration of the tank
Bo	Bond number, $\rho a r_o^2/\sigma$
C_p	specific heat of liquid at constant pressure
C_p^*	dimensionless specific heat of liquid, $C_p/C_{p,o}$
$C_{v,v}$,$C_{p,v}$	specific heats of vapor
h_{fg}	latent heat of vaporization
Ja	dimensionless parameter, $C_{p,o}T_o/h_{fg}$
k	thermal conductivity of liquid
Lh	dimensionless parameter, $p_o/(\rho_o C_{p,o} T_o)$
Ls	dimensionless parameter, $2\sigma_o/(r_o p_o)$
m_e	net mass transfer rate at the interface
Nh	dimensionless wall heat flux parameter, $q_w r_o/(k_o T_o)$
p,P	tank (vapor) pressure, liquid pressure
p^*	dimensionless tank pressure, p/p_o
q_w	wall heat flux

*Member, AIAA.

Q_v	vapor heating rate through vapor-wall boundary
R^*	vapor bubble to tank radius ratio, r_i/r_o
R_o^*	value of R^* at $t^* = 0$
r	radius
r_i, r_o	vapor bubble radius, tank radius
r^*	dimensionless radius, r/r_o
T	liquid temperature
T^*	dimensionless temperature, T/T_o
t	time
t^*	dimensionless time, $t/(r_o^2/\alpha_o)$
V_v	volume of vapor region

Greek Symbols

α	liquid thermal diffusivity, $k/(\rho C_p)$
α', β'	coefficients defined in Eq. (15)
β, β_v	coefficients of liquid and vapor thermal expansion
ε^*, τ^*	transformed coordinates defined by Eqs. (14) and (15)
κ_v	isothermal compressibility of vapor
ρ, ρ_v	liquid density, vapor density
ρ^*	dimensionless liquid density, ρ/ρ_o
σ	surface tension

Subscripts

o	liquid property evaluated at the initial condition
s	evaluated at liquid-vapor interface
v	evaluated in vapor region
w	evaluated at tank wall

Introduction

The thermal environment in space can result in heat transfer through the thermal control system and increase the pressure of a cryogenic storage system. It is required that the tank be always kept within a specified operating pressure during the entire space mission. Thus, knowledge of self-pressurization of a cryogenic fluid storage system is of great importance in the planning of space missions. Generally, the homogeneous model, which assumes a uniform temperature in liquid and vapor phases, is used as a baseline to predict the tank pressure rise rate. An analysis of pressure control based on the homogeneous model has been performed by Lin, et al.[1] Ground experiments with liquid hydrogen (LH_2) have shown that the actual pressure rise rate spans a range from about 1[2] to more than 10 times[3] faster than the homogeneous model predictions for a well insulated tank. This is due to thermal stratification in the liquid region which results in a subcooled bulk liquid and due to evaporation at interface.

In a microgravity environment, the liquid-vapor interface is principally determined by the surface tension force. The interface configuration also depends on the fluid properties, tank geometry, and liquid fill level. Usually, Bond number (Bo) and contact angle are used to characterize the interface configuration. Figure 1(a) shows the representative liquid-vapor configuration of a wetting fluid in a spherical tank for $Bo < 1$. The interface configuration on the ground where $Bo >> 1$ is shown in Fig. 1(b) for comparison. For the tank with fully wetted wall, all the heat can be transferred from the tank wall to only the liquid region which is then superheated. Pressure increase is due to liquid thermal expansion and mass transfer at the liquid-vapor interface. This paper presents a theoretical solution of thermal stratification and self-pressurization of a spherical LH_2 storage tank in a microgravity environment. Liquid is treated as a compressible fluid such that the effect of thermal expansion on the solution is taken into account. The effects of tank size, liquid fill level, and wall heat flux on the pressure rise and liquid superheat are investigated.

Problem Formulation

The physical system considered and coordinates are shown in Fig. 1(a). A spherical tank of radius r_o is partially-filled with a liquid. A vapor bubble of radius r_i is assumed to be located at the center of the tank such that the tank wall and the liquid-vapor interface form two concentric spheres. The vapor bubble configuration is representative to that of a wetting fluid in microgravity condition for $Bo < 1$. The fluid in both phases is initially at rest and at a uniform saturated temperature T_o corresponding to the vapor pressure p_o. The tank wall is subjected to a uniform and constant heat flux q_w.

Vapor Region

The vapor region is assumed to be at a uniform temperature. The pressure change rate of this homogeneous vapor region can be expressed as[4]

$$\frac{dp}{dt} = \frac{(\beta_v Q_v/C_{p,v}) + m_e - \rho_v(dV_v/dt)}{\rho_v V_v \kappa_v (C_{v,v}/C_{p,v})} \qquad (1)$$

where m_e is the net mass transfer rate at the liquid-vapor interface:

$$m_e = \begin{cases} \text{evaporation rate if} & m_e > 0 \\ \text{condensation rate if} & m_e < 0 \end{cases}$$

In the present problem, there is no direct contact between vapor region and tank wall so that $Q_v = 0$. Thus, Eq. (1) becomes

$$\frac{dp}{dt} = \frac{m_e - \rho_v(dV_v/dt)}{\rho_v V_v \kappa_v (C_{v,v}/C_{p,v})} \qquad (2)$$

Equation (2) shows that the pressure change results from the mass transfer at the liquid-vapor interface and the vapor volume change.

The mass transfer is related to the liquid temperature gradient at the interface as follows:

$$m_e = \frac{\left(k \frac{\partial T}{\partial r}\right)_s \left(4\pi r_i^2\right)}{h_{fg}} \qquad (3)$$

Thus, Eq. (2) becomes

$$\frac{dp}{dt} = \frac{3\left[\left(k \frac{\partial T}{\partial r}\right)_s \frac{1}{h_{fg}} - \rho_v \frac{dr_i}{dt}\right]}{r_i \rho_v \kappa_v (C_{v,v}/C_{p,v})} \qquad (4)$$

Clearly, the calculation in the vapor region is coupled with the liquid region through the liquid temperature gradient $(\partial T/\partial r)_s$ and through the change of interface location dr_i/dt.

Liquid Region

The liquid is treated as a compressible fluid and the following assumptions are made:

(1) The thermal conductivity, k, and the latent heat of vaporization, h_{fg}, are assumed constant and fixed at the values corresponding to its initial condition. The variation of k and h_{fg} in the range of temperature and pressure of interest is negligible.

(2) All other liquid properties such as ρ, C_p, β, and σ are considered variables.

(3) The convective terms in the energy equation are neglected.

(4) Energy dissipation is neglected.

Thus, the energy equation in the liquid region is expressed as

$$\rho C_p \frac{\partial T}{\partial t} = \frac{k_o}{r^2} \frac{\partial}{\partial r}\left(r^2 \frac{\partial T}{\partial r}\right) + \beta T \frac{\partial P}{\partial t} \qquad (5)$$

It should be noted that the liquid pressure P is different from the pressure p in the vapor region because of the surface tension effect. The relation between liquid and vapor pressure is given by

$$P = p - \frac{2\sigma}{r_i} \tag{6}$$

By using Eq. (6), Eq. (5) becomes

$$\rho C_p \frac{\partial T}{\partial t} = \frac{k_o}{r^2}\frac{\partial}{\partial r}\left(r^2 \frac{\partial T}{\partial r}\right) + \beta T \frac{\partial}{\partial t}\left(p - \frac{2\sigma}{r_i}\right) \tag{7}$$

The rate of change of liquid mass is related to the mass transfer rate at the interface through the following conservation equation:

$$\frac{d}{dt}\int_{r_i}^{r_o} 4\pi r^2 \rho \, dr + 4\pi r_i^2 \left(\frac{k_o}{h_{fg}}\right)\left(\frac{\partial T}{\partial r}\right)_s = 0 \tag{8}$$

Dimensionless Formulation

Dimensionless forms of Eqs. (4), (7), and (8) can be expressed as follows:

Vapor:

$$\frac{dp^*}{dt^*} = 3\,Ja(C_{p,v}/C_{v,v})(\rho_o/\rho_v)\frac{(\partial T^*/\partial r^*)_s}{R^*(p_o\kappa_v)} - 3(C_{p,v}/C_{v,v})\frac{(dR^*/dt^*)}{R^*}\frac{1}{(p_o\kappa_v)} \tag{9}$$

Liquid:

$$\rho^* C_p^* \frac{\partial T^*}{\partial t^*} = \frac{1}{r^{*2}}\frac{\partial}{\partial r^*}\left(r^{*2}\frac{\partial T^*}{\partial r^*}\right) + Lh(\beta T)\frac{\partial}{\partial t^*}\left(p^* - \frac{Ls}{R^*}\right) \tag{10}$$

$$\frac{d}{dt^*}\int_{R^*}^{1} r^{*2}\rho^* \, dr^* + Ja\,R^{*2}\left(\frac{\partial T^*}{\partial r^*}\right)_s = 0 \tag{11}$$

where the nondimensional variables are defined in the nomenclature.

Initial and Boundary Conditions

The tank fluid is assumed to be initially at rest at a saturated pressure p_o corresponding to an interface temperature T_o. In the present study, the liquid temperature is assumed to be uniform and equal to T_o. Thus, the initial conditions are:

$$\begin{cases} T^* = 1 \\ p^* = 1 \end{cases} \quad \text{at } t^* = 0 \text{ and } R_o^* \le r^* \le 1 \tag{12}$$

The tank wall is subjected to a uniform and constant heat flux q_w. The boundary condition at the tank wall is

$$\left(\frac{\partial T^*}{\partial r^*}\right)_w = \frac{q_w r_o}{k_o T_o} = Nh \quad \text{at } r^* = 1 \text{ for } t^* > 0 \tag{13}$$

It is noted that the temperature, $T_s^*(t^*)$, is equal to the saturation temperature corresponding to the instantaneous vapor pressure. The instantaneous location of the interface, $R^*(t^*)$, and its temperature, $T_s^*(t^*)$, must satisfy Eqs. (9) and (11) simultaneously.

Coordinate Transformation

Near the tank wall and the liquid-vapor interface, temperature gradients are expected to be large. Grid points should be clustered in these regions when the problem is solved numerically. Transformations are used which lead to a uniformly spaced grid in the computational plane while points in physical plane

are unequally spaced. Also, the interface location is moving due to the liquid thermal expansion, vapor compression, and mass transfer at the interface. The fixed number of grid points on the interior are scaled to the motion of the boundary to provide adequate resolution. In order to accomplish the above two purposes, the following formulations are proposed by using the Roberts transformation[5]:

$$\tau^* = t^* \tag{14}$$

$$\varepsilon^* = \varepsilon^*(r^*,t^*) = \alpha' + (1 - \alpha') \times \frac{\ln\left[\dfrac{\beta' + (2\alpha' + 1)(r^* - R^*)/(1 - R^*) - 2\alpha'}{\beta' - (2\alpha' + 1)(r^* - R^*)/(1 - R^*) + 2\alpha'}\right]}{\ln\left[\dfrac{(\beta' + 1)}{(\beta' - 1)}\right]} \tag{15}$$

where R^* is a function of t^* and $\beta' > 1$. Equations (14) and (15) will transform an unequally-spaced physical plane (r^*,t^*) into a uniformly spaced grid in the computational plane (ε^*,τ^*). If $\alpha' = 0$ the mesh will be refined near $r^* = 1$ only, whereas, if $\alpha' = 1/2$ the mesh will be refined equally near $r^* = 1$ and $r^* = R^*$. If the stretching parameter β' is closer to 1, the meshes are more clustered. In the present study, the values of α' and β' used are 0.5 and 1.02, respectively.

Based on this transformation, Eqs. (9) to (11) become

Vapor:

$$\frac{dp^*}{d\tau^*} = 3\,Ja\frac{C_{p,v}}{C_{v,v}}\frac{\rho_o}{\rho_v}\frac{\left(\dfrac{\partial T^*}{\partial \varepsilon^*}\right)_s}{R^*(p_o\kappa_v)}\left(\frac{\partial \varepsilon^*}{\partial r^*}\right)_s - 3\left(\frac{C_{p,v}}{C_{v,v}}\right)\frac{\dfrac{dR^*}{dt^*}}{R^*}\frac{1}{p_o\kappa_v} \tag{16}$$

Liquid:

$$\rho^* C_p^* \frac{\partial T^*}{\partial \tau^*} = \left(\frac{1}{r^{*2}}\frac{\partial \varepsilon^*}{\partial r^*}\right)\frac{\partial}{\partial \varepsilon^*}\left[\left(r^{*2}\frac{\partial \varepsilon^*}{\partial r^*}\right)\frac{\partial T^*}{\partial \varepsilon^*}\right] - \rho^* C_p^*\frac{\partial \varepsilon^*}{\partial t^*}\frac{\partial T^*}{\partial \varepsilon^*} + Lh(\beta T)\frac{\partial}{\partial \tau^*}\left(p^* - \frac{Ls}{R_o^*}\right) \tag{17}$$

$$\frac{d}{d\tau^*}\int_0^1 r^{*2}\rho^*\, d\varepsilon^* + JaR^{*2}\left(\frac{\partial T^*}{\partial \varepsilon^*}\right)_s\left(\frac{\partial \varepsilon^*}{\partial r^*}\right)_s = 0 \tag{18}$$

where

$$r^* = (1 - R^*) \times \frac{(\beta' + 2\alpha')\left(\dfrac{\beta' + 1}{\beta' - 1}\right)^{(\varepsilon^* - \alpha')/(1-\alpha')} - \beta' + 2\alpha'}{(2\alpha' + 1)\left[1 + \left(\dfrac{\beta' + 1}{\beta' - 1}\right)^{(\varepsilon^* - \alpha')/(1-\alpha')}\right]} + R^* \tag{19}$$

$$\frac{\partial \varepsilon^*}{\partial t^*} = \frac{\dfrac{2\beta'(1 - \alpha')(2\alpha' + 1)}{\ln\left(\dfrac{\beta' + 1}{\beta' - 1}\right)}}{\beta'^2 - \left[\left(\dfrac{r^* - R^*}{1 - R^*}\right)(2\alpha' + 1) - 2\alpha'\right]^2} \times \left[\frac{-\left(\dfrac{dR^*}{dt^*}\right)(1 - r^*)}{(1 - R^*)^2}\right] \tag{20}$$

$$\frac{\partial \varepsilon^*}{\partial \tau^*} = \frac{\dfrac{2\beta'(1-\alpha')(2\alpha'+1)}{\ln\left(\dfrac{\beta'+1}{\beta'-1}\right)}}{\beta'^2 - \left[\left(\dfrac{r^*-R^*}{1-R^*}\right)(2\alpha'+1) - 2\alpha'\right]^2} \times \frac{1}{1-R^*} \tag{21}$$

Also, the boundary condition, Eq. (13), transforms to

$$\left(\frac{\partial T^*}{\partial \varepsilon^*}\right)_w = \frac{Nh}{\left(\dfrac{\partial \varepsilon^*}{\partial \tau^*}\right)_w} \tag{22}$$

Solution Algorithm

The governing equations (Eqs. (16) to (18)) are placed in finite-difference forms, along with the initial and boundary conditions. The Crank-Nicolson implicit scheme is chosen as the finite-difference method of solution. The thermodynamic and transport properties of the fluid are obtained by using the GASP code.[6]

An iterative procedure is necessary to determine the required location of the interface $R^*(t^*)$ and the interface temperature $T_s^*(t^*)$. The required R^* and T_s^* should satisfy that the calculated tank pressure based on Eqs. (16) to (18) is equal to the saturation pressure corresponding to T_s^*. Assuming the solutions of $\tau^* = \tau^{*n}$ are known (where n represents the n^{th} time step), the general procedure of carrying out the numerical computations for $\tau^* = \tau^{*n+1}$ is listed below:

(1) For a given guessed value of $R^*(\tau^{*n+1})$,

   (a) Guess a value for the interface temperature $T_s^*(\tau^{*n+1})$.

   (b) Solve Eq. (17) for liquid temperature distribution.

   (c) Check Eq. (18) for liquid mass conservation. If satisfied, go to Step (2). Otherwise, adjust the guessed value of $T_s^*(\tau^{*n+1})$ and repeat Steps 1(b) and (c).

(2) Solve Eq. (16) for vapor pressure $p^*(\tau^{*n+1})$.

(3) Check if the difference between the vapor pressure $p^*(\tau^{*n+1})$ obtained in Step (2) and the saturation pressure corresponding to the interface temperature $T_s^*(\tau^{*n+1})$ obtained in Steps 1(a) to (c) is less than 10^{-4}.

   (a) If yes, the current solutions are the solutions for $\tau^* = \tau^{*n+1}$. Set $n = n+1$ and go to Step (1) to start the calculations for the next time step.

   (b) If no, adjust the guessed value of $R^*(\tau^{*n+1})$ and repeat the Steps (1) to (3).

Results and Discussion

The mathematical modeling described in the previous section shows that the solution of the problem depends on the fluid type and the parameters: t^*, Ja, Lh, Ls, R_o^*, and Nh. For a given fluid and a given initial conditions, the parameters Ja and Lh are specified. The pressure and temperature changes in the tank at any time t^* are controlled only by the parameters Ls, R_o^*, and Nh, which characterize the effects of tank size (r_o), liquid fill level (r_i/r_o), and wall heat flux (q_w). For liquid hydrogen system of practical interest, the parameter Ls, is less than 10^{-6}. Therefore, the term containing Ls in comparison to other terms in Eq. (17) is neglected. In the present study, a liquid hydrogen system initially in a homogeneous state of 1 atm is considered. The ranges of R_o^* and Nh are selected to be

$$0.4 \le R_o^* \le 0.9 \quad \text{and} \quad 0.05 < Nh < 0.5$$

Figure 2 shows that, for a given R_o^* the dimensionless pressure rise is higher for increasing values of Nh. Thus, for a given tank size and liquid fill level, tank pressure increases faster for higher wall heat flux q_w. The pressure rise is due to the combined effects of the thermal expansion of the liquid and the mass transfer at the interface. The pressure rise rate as predicted by using a homogeneous model is also included in Fig. 2 for comparison. The results show that tank pressure rise rate can be slower than the homogeneous rate if there is no direct contact between tank wall and vapor region and heat is transferred to the liquid region only. This is due to significant liquid superheating.

Figure 3 shows the effect of liquid fill level on the tank pressure rise. For a given Nh, tank pressure increases faster for lower fill level (higher R_o^*) than higher fill level (lower R_o^*) except for the initial time period. Before the effect of wall heat flux reaches the interface, tank pressure change is basically governed by the volume change of vapor region. Therefore, the equation of state yields

$$\frac{\Delta p}{p} \propto \frac{-\Delta V_v}{V_v} \qquad (23)$$

Since vapor volume change ($-\Delta V_v$) due to liquid thermal expansion is approximately the same for both low and high fill levels, Eq. (23) shows that for a given tank the effect of liquid thermal expansion on the tank pressure rise should be more significant for higher liquid fill level. This liquid thermal expansion causes a higher pressure rise for higher fill level during the initial time period. Thermal expansion not only causes vapor compression to increase vapor pressure but also causes negative temperature gradient at the interface to induce interface condensation. Thus, liquid temperature near the interface region increases. This impedes heat transfer from the wall to the interface to cause evaporation. Therefore, after the initial time period in which thermal expansion effect is dominant, the pressure rise becomes faster for lower fill level (as shown in Fig. 3) because heat has been transferred to the interface to cause evaporation. This phenomena can be better explained by using Fig. 4, which shows the effect of R_o^* on the temperature gradient at the interface for a given Nh. For low fill level such as $R_o^* = 0.9$, the change in the interface temperature due to the thermal expansion of liquid and compression of vapor is negligible. The temperature gradient at the interface is always positive and results in evaporation. On the other hand, for high fill level such as $R_o^* = 0.4$, the pressure increases mainly due to the liquid thermal expansion and vapor compression. The interface temperature increases because of the increase in pressure, resulting in a negative temperature gradient near the interface and vapor condensation. It is noted that the oscillations of the data in Fig. 4 is probably related to the accuracy in calculations of fluid and thermodynamic properties in GASP, which basically uses a curve-fitting technique.

For low liquid fill level and low wall heat flux, the liquid compressibility and fluid property variations may be neglected. Under these conditions, the temperature distribution in liquid region can be predicted approximately by using the theoretical solution for transient conduction in a semi-infinite solid with constant surface heat flux, as long as the interface temperature has not responded to the effect of wall heat flux.

For a given R_o^* and Nh, liquid superheat increases with time. Figures 5 and 6 show that the wall superheat ΔT^*, where $\Delta T^* = T_w^* - T_s^*$, approaches an asymptotic value for a given R_o^* and Nh. This asymptotic value of wall superheat, $(\Delta T^*)_{max}$, increases with increasing Nh and decreasing R_o^*. A simplified correlation which is developed for maximum wall superheat as a function of R_o^* and Nh using numerical results is given as follows:

$$(\Delta T^*)_{max} = 0.55\left(1 - R_o^*\right)^{0.89} Nh \qquad (24)$$

for $(1 - R_o^*)Nh < 0.15$. For values of $(1 - R_o^*)Nh$ greater than 0.15, Eq. (24) overpredicts $(\Delta T^*)_{max}$. It should be noted that, although pressure rise rate is slower for a tank with higher liquid fill level (smaller R_o^*), the maximum liquid superheat $(\Delta T^*)_{max}$ is greater. A superheated liquid represents a metastable condition and may lead to a pressure spike either due to boiling or flashing of liquid. Therefore, Eq. (24) may provide useful information for the system designer to avoid the occurrence of pressure spikes due to liquid boiling, once the incipient boiling temperature is known.

Conclusion

An analysis of thermal stratification and self-pressurization of a spherical liquid hydrogen tank with a spherical vapor bubble located at the center has been performed. The liquid-vapor interface configuration considered corresponds to that of a wetting liquid in a microgravity condition, i.e., Bo < 1. Based on the assumptions and conditions considered, the present study draws the following conclusions:

- For a tank with fully-wetted wall, the pressure rise rate can be lower than the homogeneous pressure rise rate because of superheat of the liquid region.

- For a given liquid fill level, dimensionless tank pressure rise is higher for increasing values of Nh. Thus, for a given tank size and fill level, higher wall heat flux results in a higher pressure increase.

- Tank pressure increases faster initially for a higher fill level because of the significant effect of liquid thermal expansion. However, after a period of time, the pressure increase becomes faster for a lower fill level tank because of the interface evaporation.

- Liquid thermal expansion tends to cause vapor condensation and wall heat flux tends to cause liquid evaporation at the interface. The combined effects determine the direction of mass transfer at the interface.

- Liquid superheat increases with increasing wall heat flux and liquid fill level and approaches an asymptotic value. For a tank with $(1 - R_o^*)Nh < 0.15$, a simplified correlation, i.e., Eq. (24), is developed for the maximum wall superheat using the numerical results.

References

1. Lin, C.S., Van Dresar, N.T., and Hasan, M.M.: "A Pressure Control Analysis of Cryogenic Storage Systems," AIAA Paper 91-2405, June 1991 (also, NASA TM-104409).

2. Hasan, M.M., Lin, C.S., and Van Dresar, N.T.: "Self-Pressurization of a Flightweight Liquid Hydrogen Storage Tank Subjected to Low Heat Flux," NASA TM-103804, 1991.

3. Liebenberg, D.H., and Edeskuty, F.J.: "Pressurization Analysis of a Large-Scale Liquid Hydrogen Dewar," International Advances in Cryogenic Engineering, K.D. Timmerhaus, ed., Plenum Press, Vol. 10 (sections M-U), 1965, pp. 284-289.

4. Brown, J.S.: "Vapor Condensation on Turbulent Liquid," Ph.D. Dissertation, Dept. of Mechanical Engineering, Massachusetts Institute of Technology, 1991.

5. Roberts, G.O.: "Computational Meshes for Boundary Layer Problems," Proceedings of the Second International Conference on Numerical Methods in Fluid Dynamics, M. Holt, ed., Springer-Verlag, New York, 1971, pp. 171-177.

6. Hendricks, R.C., Baron, A.K., and Peller, I.C.: "GASP—A Computer Code for Calculating the Thermodynamic and Transport Properties for Ten Fluids: Para Hydrogen, Helium, Neon, Methane, Nitrogen, Carbon Monoxide, Oxygen, Fluorine, Argon, and Carbon Dioxide," NASA TN D-7808, 1975.

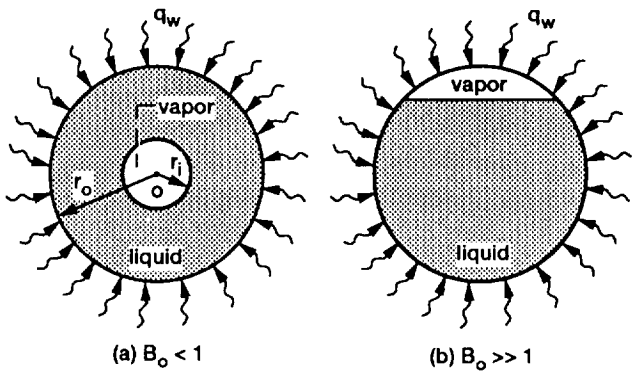

Figure 1.—Physical system and coordinates.

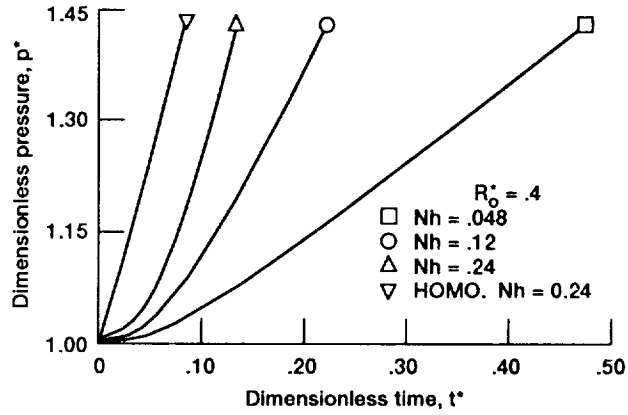

Figure 2.—Pressure rise as a function of time for various heat flux levels.

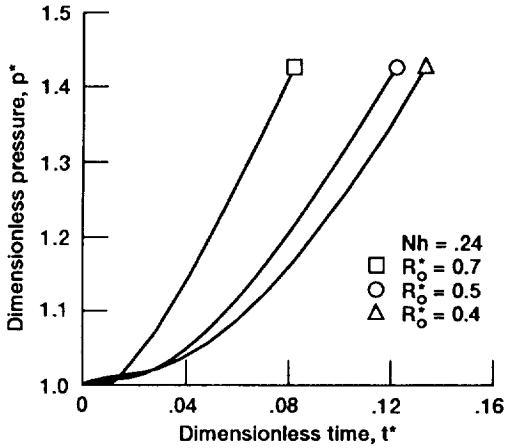

Figure 3.—Pressure rise as a function of time for various fill levels.

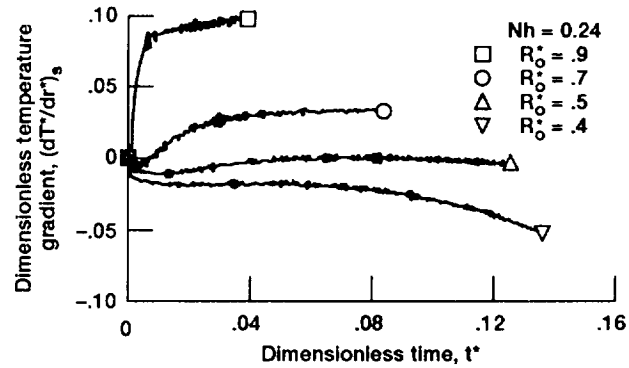

Figure 4.—Liquid temperature gradient at interface as a function of time for various fill levels.

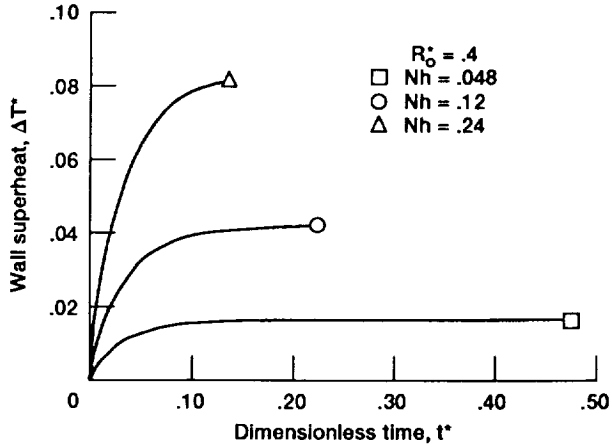

Figure 5.—Wall superheat as a function of time for various heat flux levels.

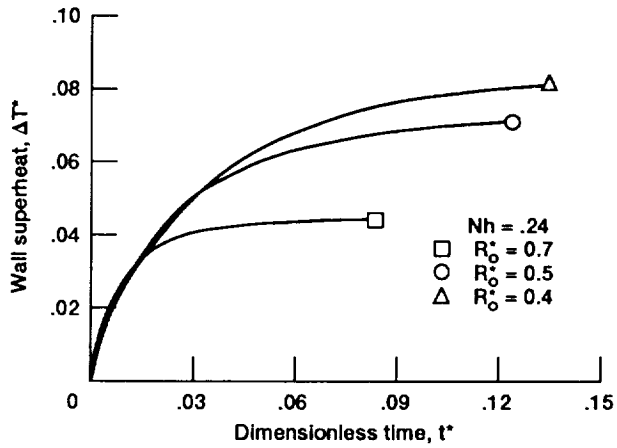

Figure 6.—Wall superheat as a function of time for various fill levels.

REPORT DOCUMENTATION PAGE

Form Approved
OMB No. 0704-0188

Public reporting burden for this collection of information is estimated to average 1 hour per response, including the time for reviewing instructions, searching existing data sources, gathering and maintaining the data needed, and completing and reviewing the collection of information. Send comments regarding this burden estimate or any other aspect of this collection of information, including suggestions for reducing this burden, to Washington Headquarters Services, Directorate for information Operations and Reports, 1215 Jefferson Davis Highway, Suite 1204, Arlington, VA 22202-4302, and to the Office of Management and Budget, Paperwork Reduction Project (0704-0188), Washington, DC 20503.

1. AGENCY USE ONLY (*Leave blank*)	2. REPORT DATE	3. REPORT TYPE AND DATES COVERED
	1991	Technical Memorandum

4. TITLE AND SUBTITLE

Self-Pressurization of a Spherical Liquid Hydrogen Storage Tank in a Microgravity Environment

5. FUNDING NUMBERS

WU-593-21

6. AUTHOR(S)

C.S. Lin and M.M. Hasan

7. PERFORMING ORGANIZATION NAME(S) AND ADDRESS(ES)

National Aeronautics and Space Administration
Lewis Research Center
Cleveland, Ohio 44135-3191

8. PERFORMING ORGANIZATION REPORT NUMBER

E-6759

9. SPONSORING/MONITORING AGENCY NAMES(S) AND ADDRESS(ES)

National Aeronautics and Space Administration
Washington, D.C. 20546-0001

10. SPONSORING/MONITORING AGENCY REPORT NUMBER

NASA TM-105372
AIAA-92-0363

11. SUPPLEMENTARY NOTES

Prepared for the 30th Aerospace Sciences Meeting and Exhibit sponsored by the American Institute of Aeronautics and Astronautics, Reno, Nevada, January 6-9, 1992. C.S. Lin, Analex Corporation, 3001 Aerospace Parkway, Brook Park, Ohio 44142; M.M. Hasan, NASA Lewis Research Center. Responsible person, C.S. Lin, (216) 977-0138.

12a. DISTRIBUTION/AVAILABILITY STATEMENT

Unclassified - Unlimited
Subject Category 34

12b. DISTRIBUTION CODE

13. ABSTRACT (*Maximum 200 words*)

Thermal stratification and self-pressurization of partially filled liquid hydrogen (LH_2) storage tanks under microgravity condition is theoretically studied. The tank is spherical and is subjected to a uniform and constant wall heat flux. It is assumed that a vapor bubble is located in the tank center such that the liquid-vapor interface and tank wall form two concentric spheres. This vapor bubble represents an idealized configuration of a wetting fluid in microgravity conditions. Dimensionless mass and energy conservation equations for both vapor and liquid regions are numerically solved. Coordinate transformation is used to capture the interface location which changes due to liquid thermal expansion, vapor compression, and mass transfer at liquid-vapor interface. The effects of tank size, liquid fill level, and wall heat flux on the pressure rise and thermal stratification are investigated. Liquid thermal expansion tends to cause vapor condensation and wall heat flux tends to cause liquid evaporation at the interface. The combined effects determine the direction of mass transfer at the interface. Liquid superheat increases with increasing wall heat flux and liquid fill level and approaches an asymptotic value. A simplified correlation is developed for the maximum wall superheat as a function of system parameters using the numerical results.

14. SUBJECT TERMS	15. NUMBER OF PAGES
	10
	16. PRICE CODE
	A03

17. SECURITY CLASSIFICATION OF REPORT	18. SECURITY CLASSIFICATION OF THIS PAGE	19. SECURITY CLASSIFICATION OF ABSTRACT	20. LIMITATION OF ABSTRACT
Unclassified	Unclassified	Unclassified	